Chapter 4

Thermoelectric Energy Harvesting

Douglas Paul

Additional information is available at the end of the chapter

http://dx.doi.org/10.5772/57092

1. Introduction

The generation of electrical energy from thermal energy was originally discovered by Thomas Johann Seebeck in 1822 when he first demonstrated that a thermoelectric voltage was produced after providing a temperature difference across two materials. Jean Charles Athanase Peltier then demonstrated in 1834 that the application of a current could be used to pump heat, an effect with great potential for refrigeration. It was not until the 1850s that Lord Kelvin worked out the physics of the Seebeck and Peltier effects attributing the reversible heat flow discovered by Peltier must have an entropy associated with it and the Seebeck coefficient was a measure of the entropy associated with the electric current. Further developments in the theoretical understanding of thermoelectrics required quantum mechanics. The efficiency of the thermoelectric generation process was derived in 1911 by Edmund Altenkirch.

2. Fundamental physics

Before describing and deriving the main thermodynamic properties and equations, it is worthwhile having a brief review of the key parts of physics required for thermoelectrics. One of the first effects that will be used to derive the thermoelectric efficiency is Joule's law of heating. Joule was the first to demonstrate that any current passing through a resistor produces an amount of heat (Fig. 1(a)). Specifically the heat, Q (as a power i.e. energy / time) generated by passing a current, I though a resistance, R is given by Joule's first law

$$Q = I^2 R \tag{1}$$

It should be clear that thermoelectrics have heat being transported through a range of materials and some understanding of the transport of that heat is required. The heat generated by any process will be transported through a material driven by any temperature

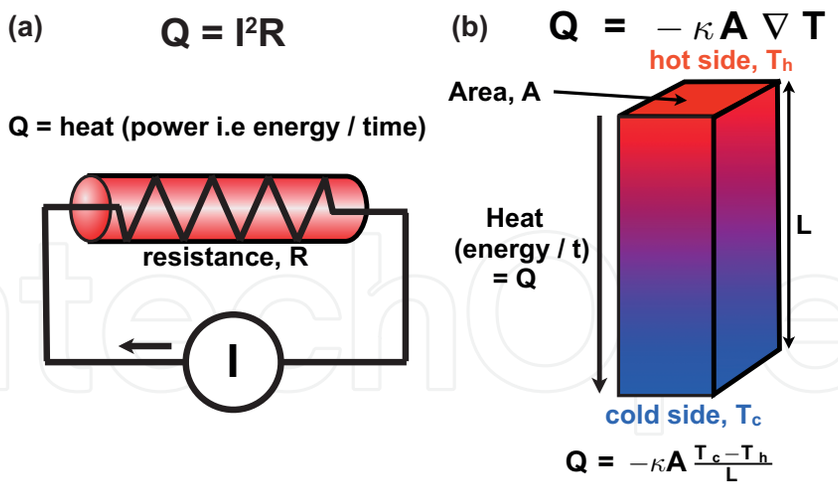

Figure 1. (a) The heat power generated by Joule heating of a resistance, R with current, I flowing through the resistance. (b) The thermal transport through a rod of area, A, length L and thermal conductivity κ as defined by Fourier's law of thermal transport.

gradients along the material (Fig. 1(b)). This is given by Fourier's law of heat transport which states for a material with area A and thermal conductivity κ that

$$Q = -\kappa A \nabla T \left(= -\kappa A \frac{T_c - T_h}{L} \text{for 1D transport along a length, } L \right) \tag{2}$$

Strictly speaking the heat transport could be in multiple directions in a complex material with a range of different thermal conductivities in different directions but for most thermoelectrics systems, the designs attempt to keep the heat flow simple by using 1 dimensional constructs. The right hand term of equation 2 is the equation for 1D heat transport which is predominantly the one used in thermoelectric devices and modules.

After discussing the generation and transport of heat, we can now discuss the thermoelectric effects. It is far easier to understand the Peltier effect and so this will be discussed before the Seebeck effect. We need to consider two materials in a thermocouple connected between a hot reservoir of temperature, T_h and a cold reservoir of temperature T_c (Fig. 2(a)). To produce the Peltier effect, a current has to be applied and so Fig. 2(a) demonstrate the system with the current being applied to the ends of material 2. The Peltier coefficient, Π, for this system is given by

$$\Pi = \frac{Q}{I} \tag{3}$$

The units of Π are the Volt since heat divided by current is Watts divided by Amps. The physics of what is going on is relatively simple. The Peltier coefficient is the heat energy carried by each electron per unit charge and time from the hot reservoir to the cold reservoir.

The Seebeck effect requires a similar circuit to be constructed but this time, the gap in material two is left open circuit (Fig. 2(b)). The open circuit voltage is proportional to

http://dx.doi.org/10.5772/57092

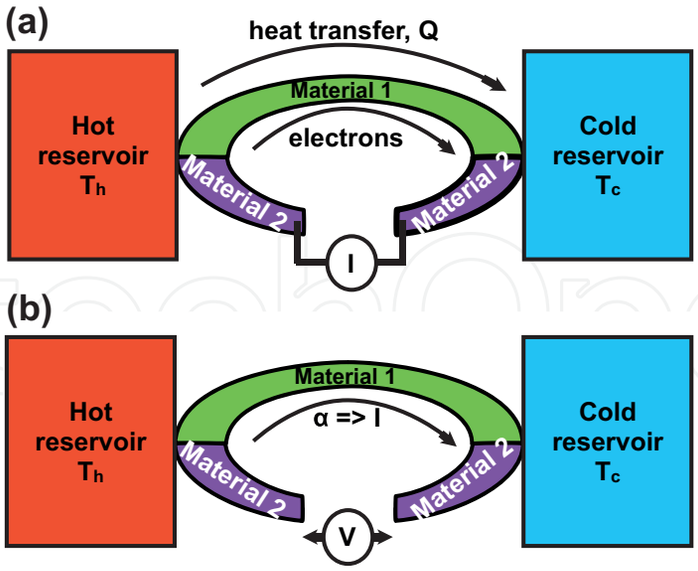

Figure 2. (a) The thermocouple system between two heat reservoirs required to demonstrate the Peltier effect (b) The thermocouple system between two heat reservoirs required to demonstrate the Seebeck effect.

$(T_h - T_c) = \Delta T$ and the constant of proportionality is called the Seebeck coefficient, α. More generally the Seebeck coefficient is defined as

$$\alpha = \frac{\mathrm{d}V}{\mathrm{d}T} \tag{4}$$

The units for the Seebeck coefficient are V/K. The Seebeck coefficient is 1/q times the entropy (Q/T) transported with each electron where q is the electron charge. Hence the Peltier effect is just each electron in the electrical current transferring an amount of heat from one reservoir to the other i.e. a heat pump.

To calculate the Seebeck or Peltier coefficients from theory requires one to solve the Boltzmann transport equation in the relaxation time approximation. This is beyond the scope of this text but a full derivation can be found in a range of solid state text books including [1]. From this approach, the Seebeck coefficient can be written in terms of the energy of an electron, E, Boltzmann's constant, k_B, the Fermi level in the thermoelectric material, E_F and the momentum relaxation time, τ, as

$$\alpha = -\frac{k_B}{q}\int \frac{(E - E_F)}{k_B T}\frac{\sigma(E)}{\sigma}\mathrm{d}E \tag{5}$$

where the electrical conductivity

$$\sigma = \int \sigma(E)dE = q\int g(E)\mu(E)f(E)(1 - f(E))\mathrm{d}E \tag{6}$$

The functions are the density of states, $g(E)$, the carrier mobility, $\mu(E)$ and the Fermi function, $f(E)$. The best thermoelectric materials are always semiconductors and so the equation for the Seebeck coefficient can be integrated over either the conduction band or the valence band to find the solution for n-type semiconductors and p-type semiconductors respectively. If we only consider electrons in the conduction band for energies above the conduction band edge, E_c then we have

$$\alpha = -\frac{k_B}{q}\left[\frac{(E_c - E_F)}{k_B T} + \frac{\int_0^\infty \frac{(E-E_c)\sigma(E)\mathrm{d}E}{k_B T}}{\int_0^\infty \sigma(E)\mathrm{d}E}\right] \quad \text{for } E > E_c \tag{7}$$

This equation is still quite complex and it is difficult to see exactly how to optimise thermoelectric materials. Cutler and Mott [2] realised a more useful form for the Seebeck coefficient. By differentiating the Fermi function it is easy to show that $f(1-f) = -k_B T \frac{\mathrm{d}f}{\mathrm{d}E}$ and then expanding $g(E)\mu(E)$ in a Taylor's series around $E = E_F$ it can be shown that

$$\alpha = -\frac{\pi^2}{3q} k_B^2 T \left[\frac{d \ln(\mu(E)g(E))}{dE}\right]\Bigg|_{E=E_F} \tag{8}$$

This equation is only valid for degenerately doped material, that is material that has doping above the Mott criteria and so the Fermi energy is greater than the conduction band edge. The doping density, n_c given by the Mott criteria is

$$n_c \approx \left(\frac{0.27}{a_B^*}\right)^3 \tag{9}$$

where a_B^* is the effective Bohr radius given by

$$a_B^* = \frac{\epsilon_0 \epsilon_r h^2}{\pi m^* q^2} \tag{10}$$

with ϵ_0 the permittivity of free space ($8.85 \times 10^{-}12$ Fm^{-1}), ϵ_r the dielectric constant of the semiconductor, h is Planck's constant and m^* is the effective mass of the charge carrier in the semiconductor. In metal-insulator theory this makes the degenerate semiconductor doped above Mott criteria metallic. The Cutler and Mott equation 8 now starts to suggests methods for optimising thermoelectric materials. Materials where the mobility and/or the density of states are varying by large amounts around the Fermi level have high Seebeck coefficients.

Further insights into how to increase the Seebeck coefficient can be found by taking the approach by Ziman [1]. If we ignore energy dependent scattering so that the momentum

http://dx.doi.org/10.5772/57092

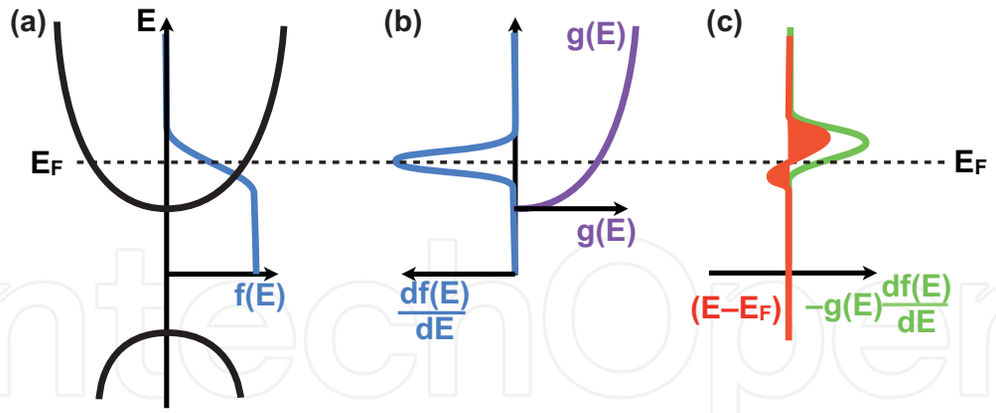

Figure 3. (a) The Fermi function demonstrating the carrier occupation as a function of energy for a degenerately doped semiconductor. (b) The first derivative of the Fermi function with respect to energy and also the density of states for the same semiconductor. (c) The product of the terms in (b) times $(E - E_F)$ which is related to the Seebeck coefficient as detailed in the text. It is the asymmetry between the two red areas above and below the Fermi energy that determines the magnitude of the Seebeck coefficient of the semiconductor.

relaxation time is given by $\tau(E)$ and the electron velocity by $v(E)$ then the electrical conductivity can be written as

$$\sigma = \frac{q^2}{3} \int \tau(E) v^2(E) \left[-g(E) \frac{\mathrm{d}f}{\mathrm{d}E} \right] \mathrm{d}E \tag{11}$$

Zimen then demonstrated that the Seebeck coefficient can be written as

$$\alpha = \frac{q^2}{3T\sigma} \int \tau(E) v^2(E) \left[-g(E) \frac{\mathrm{d}f}{\mathrm{d}E} \right] (E - E_F) \mathrm{d}E \tag{12}$$

Fig. 3 provides a graphical plot of the terms $\left[-g(E) \frac{\mathrm{d}f}{\mathrm{d}E} \right] (E - E_F)$ in this equation. With this approach by Ziman, σ, τ and v are all constant and it is therefore the asymmetry between the value of this term above and below the Fermi level that determines the magnitude of the Seebeck coefficient. This results is important when low dimensional structures are considered as large discontinuities of the density of states can potential provide significant enhancements to the Seebeck coefficient.

William Thomson (Lord Kelvin), realised that the Seebeck coefficient varies with temperature (Fig. 4) and so heat is both absorbed and generated in the thermocouples shown in Fig. 2. The gradient of the heat flux is then given by

$$\frac{dQ}{dx} = \beta I \frac{\mathrm{d}T}{\mathrm{d}x} \tag{13}$$

where β is the Thomson coefficient. Kelvin then derived the Kelvin relationships that hold for all materials which are

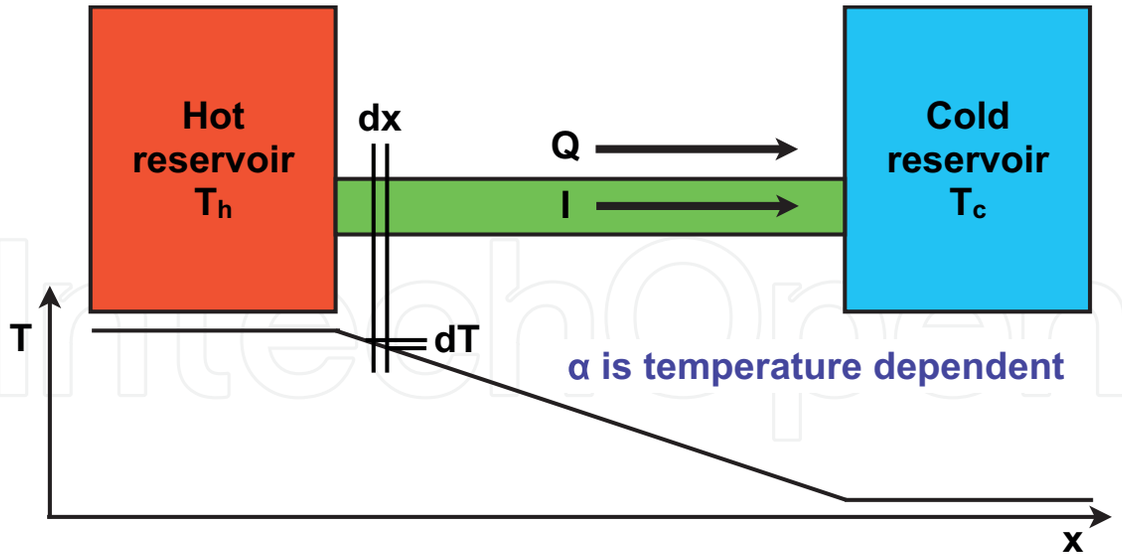

Figure 4. The Thomson coefficient is required as there will be a temperature dependence along any thermoelectric material connected to two heat reservoirs at different temperatures and this produces different Seebeck coefficients along the thermoelectric material. In this diagram the Seebeck coefficient varies along the x-direction i.e. $\alpha = \alpha(x)$

$$\Pi = \alpha T \tag{14}$$

$$\beta = T\frac{\mathrm{d}\alpha}{\mathrm{dT}} \tag{15}$$

The Peltier and Thomson coefficients are extremely difficult to measure experimentally but the Seebeck coefficient is relatively easy as it only requires a voltage measurement as a function of ΔT across the thermoelectric material. The Kelvin relationships therefore allow the measurement of the Seebeck effect to obtain the Peltier and Thomson coefficients.

3. Thermodynamic efficiency

We are about to derive the thermodynamical efficiency of thermoelectrics as first demonstrated by Altenkirch in 1911. Before undertaking this, it is sensible to review the Carnot cycle efficiency as this is the maximum efficiency for converting a given amount of thermal energy into work done. It will therefore set a maximum amount for any thermal system and will allow us to determine how much scope there may be for improving thermoelectric materials.

Fig. 5 shows the Carnot cycle where the input work done, W_{com} to a compressor increases the pressure of the water. This input work done is adiabatic so there is no gain or loss of heat within the complete system. The water flows from the compressor to a furnace where an amount of heat, Q_1 is input into the water at constant temperature (i.e. along an isotherm) so that the water is converted from water into dry steam. Therefore all the heat energy is being absorbed as the latent heat in this process of changing water into dry steam. The steam has a larger volume than the liquid water and so the volume increases as shown in Fig. 5(b). This

http://dx.doi.org/10.5772/57092

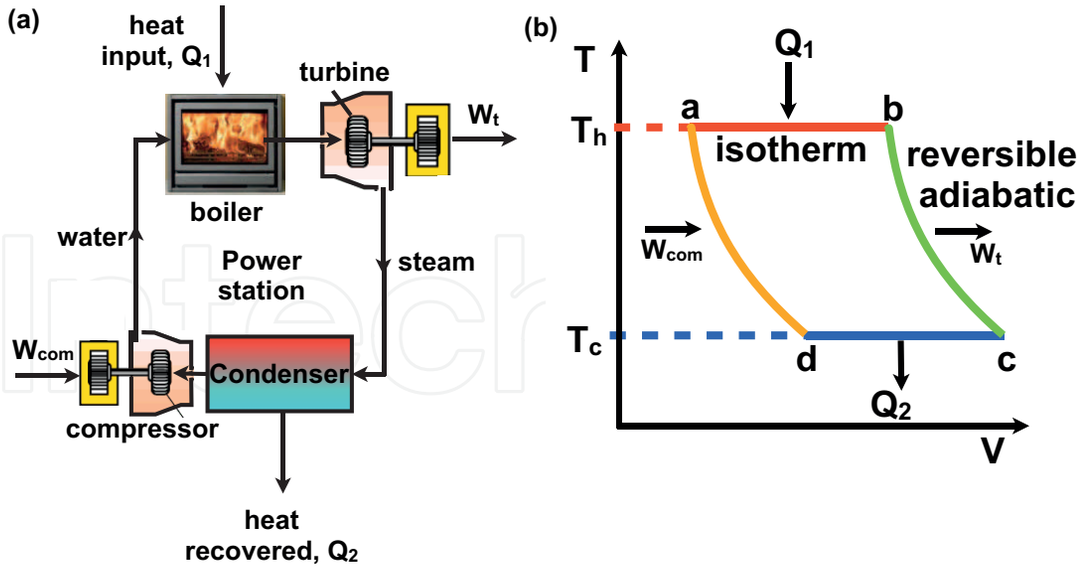

Figure 5. (a) The Carnot thermodynamical cycle showing a closed cycle water / steam system where input work, W_{com} is done of the water / steam by a compressor and the work done as output, W_t is that which is the output from a turbine. (b) The temperature-volume phase diagram for the Carnot thermodynamic cycle shown in (a).

increase in volume can be used to turn a turbine and the kinetic energy from the volume expansion can be recovered as work done on the turbine, W_t. The temperature is reduced in this process. Then to allow the cycle to start again, the steam has to be condensed into water, and the latent heat, Q_2 which is removed at constant temperature can be recovered and reused as an input. The process can then start again.

The efficiency of the Carnot cycle is given by

$$\text{Efficiency} = \eta = \frac{\text{net work output}}{\text{net work input}} = \frac{W_t - W_{com}}{Q_1} \tag{16}$$

From the first law of thermodynamics (conservation of energy), we have

$$(Q_1 - Q_2) - (W_t - W_{com}) = 0 \tag{17}$$

and so the efficiency can be rewritten as

$$\eta = \frac{Q_1 - Q_2}{Q_1} = 1 - \frac{Q_2}{Q_1} \tag{18}$$

Carnot demonstrated using the temperature versus volume diagram for the Carnot cycle (Fig. 5(b)) that the maximum efficiency is only dependent on the maximum (T_h) and minimum temperatures (T_c) in the cycle and so the maximum efficiency known as the Carnot efficiency becomes

$$\eta_c = 1 - \frac{T_c}{T_h} \tag{19}$$

The Carnot efficiency is related to the Kelvin statement of the second law of thermodynamics which states that no system operating in a closed cycle can convert all the heat absorbed from a heat reservoir into the same amount of work. This is just a statement that no thermodynamic heat engine is 100 % efficient. The equivalent Caussius statement is that no process is possible whose sole result is the transfer of heat from a colder to a hotter body when no work is done inside the system. Heat must always flow from a hotter to a colder body. Heat can only be pumped from a colder to a hotter body by undertaking work on the system. Hence the Peltier effect provides one mechanism to pump heat when a current and electrical energy provides the work.

The equation clearly demonstrates that the efficiency can be increased by decreasing T_c or increasing T_h. More correctly the larger $\Delta T = T_h - T_c$ becomes, the higher the efficiency. Therefore for practical systems, the easiest way to increase the efficiency of any heat engine is to increase the hot reservoir temperature, T_h.

We have already described how a temperature gradient across a material results in heat conduction through Fourier's law when no electrical current flows in the system. If there is an electrical current in the same direction due to the Seebeck effect then the Peltier effect will attempt to oppose the applied temperature gradient. Therefore when the heat flows through a thermoelectric material between hot and cold reservoirs (see Fig. 1(a)), we have to consider not just the Fourier heat transport but also the Peltier effect.

We therefore need to write: Heat flux per unit area = Peltier term + Fourier term

$$\frac{Q}{A} = \Pi J - \kappa \nabla T \tag{20}$$

From the Kelvin relations we have $\Pi = \alpha T$ and the current density, $J = \frac{I}{A}$. Therefore this can be rewritten as

$$Q = \alpha I T - \kappa A \nabla T \tag{21}$$

We will now derive the thermodynamic efficiency of a thermoelectric generator. Before we can generate electricity, we need to build a circuit that can deliver power to a load. Fig. 6(a) shows the basic thermoelectric circuit for generating electricity which consists of an n-type and a p-type semiconductor connected electrically in series and thermally in parallel. The output power is delivered to a load which in this case will just be a resistor, R_L. For a Peltier cooler, a similar circuit can be designed where the load is replaced by a current source or battery as demonstrated in Fig. 6(b). The thermodynamic efficiency of the thermoelectric generator is given by

http://dx.doi.org/10.5772/57092

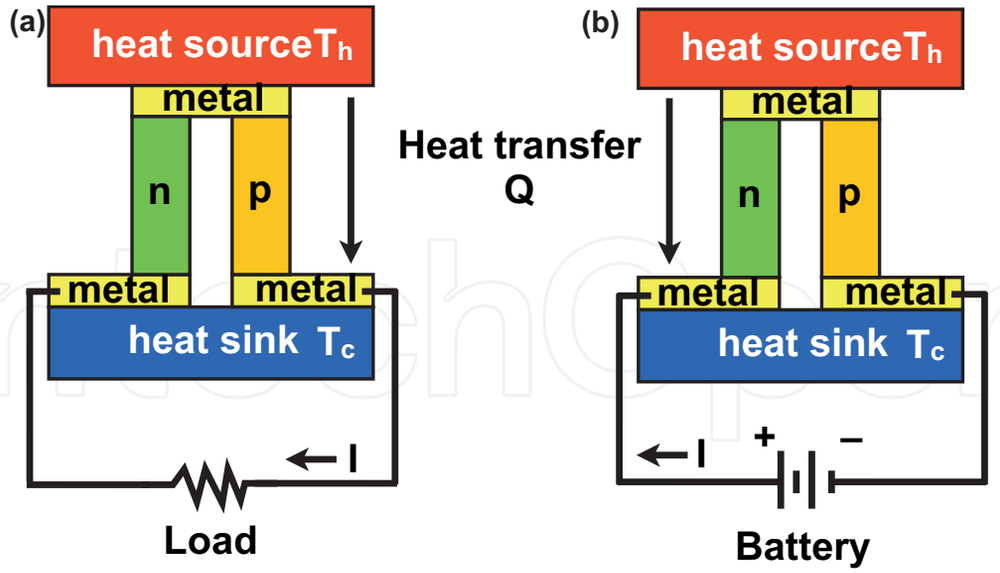

Figure 6. (a) A thermoelectric generator delivering power through current to a resistive load connected in electrical series to n- and p-type semiconductor thermoelectric materials. (b) A heat pump (or Peltier cooler) where a current is used to transport heat from the hot reservoir to the cold reservoir. By reversing the current, heat from the cold sink can be pumped by the Peltier effect to the hot sink by undertaking work.

$$\eta = \frac{\text{power supplied to load}}{\text{heat absorbed at hot junction}} \tag{22}$$

The power supplied to the load is just the Joule heating of the load resistor, R_L which is equal to I^2R_L. The heat absorbed at the hot junction is the Peltier term plus the heat withdrawn from the hot junction as described above. The Peltier heat is given by $\Pi I = \alpha I T_h$. If the resistance of the n-type and p-type semiconductor elements in series is R, then the current, I flowing in the circuit is just given by Ohm's Law as

$$I = \left(\frac{V}{R_{total}}\right) = \frac{\alpha(T_h - T_c)}{R + R_L} \tag{23}$$

The heat withdrawn from the hot junction is given by the Fourier term but as there will be Joule heating from the generated current from the Seebeck voltage, some heat will also be generated and returned to the hot junction. It is usual to assume that half of the Joule heat will be transport and half will be returned to the hot junction and so

$$Q_h = \text{Fourier - Joule heating + half Joule heating returned} \tag{24}$$

$$= \kappa A(T_h - T_c) - I^2R + \frac{1}{2}I^2R \tag{25}$$

$$= \kappa A(T_h - T_c) - \frac{1}{2}I^2R \tag{26}$$

We can now move to calculate the efficiency by combining these terms and assuming that the power supplied to the load is only through Joule heating to produce

$$\eta = \frac{\text{power supplied to load}}{\text{heat absorbed at hot junction}} \tag{27}$$

$$= \frac{\text{power supplied to load}}{\text{Peltier + heat withdrawn from hot junction } (Q_h)} \tag{28}$$

$$= \frac{I^2 R_L}{\alpha I T_h + \kappa A (T_h - T_c) - \frac{1}{2} I^2 R} \tag{29}$$

To find the maximum efficiency, this equation requires to be solved for $\frac{\mathrm{d}\eta}{\mathrm{d}\left(\frac{R_L}{R}\right)} = 0$. With a little algebra it can be shown that the solution is

$$\eta_{max} = (1 - \frac{T_c}{T_h}) \frac{\sqrt{1 + ZT} - 1}{\sqrt{1 + ZT} + \frac{T_c}{T_h}} \tag{30}$$

where $T = \frac{1}{2}(T_h + T_c)$ and the figure of merit for thermoelectrics is defined as

$$ZT = \frac{\alpha^2 \sigma}{\kappa} T \tag{31}$$

Equation 30 has two parts. The first part is just the Carnot efficiency given by $(1 - \frac{T_c}{T_h})$. The second part accounts for losses and irreversible processes which reduce as the dimensionless figure of merit, ZT, increases in value.

Fig. 7 demonstrates the Carnot efficiency and the maximum thermoelectric efficiencies for different ZTs as a function of ΔT. Also included are typically efficiencies for other thermodynamic cycles such as the Rankine and Stirling cycles for different thermal heating schemes. It is clear from this figure that thermoelectrics have significantly less efficiency today that Rankine or Stirling cycle engines. This is certainly true for power generation at the large scale. Below about 100 W, however, the Rankine and Stirling cycles become more difficult to sustain at high efficiencies and thermoelectrics have some advantages. This is mainly due to the fact that fluids effectively become more viscous (lossy) when dimensions are reduced below a certain length scale. A second major advantage of the thermoelectric generators is that they have no moving mechanical parts and are therefore significantly more reliable than Rankine or Stirling cycle engines which have compressors and turbines. Indeed, this is the major reason NASA used radioisotope thermoelectric generators for the Voyager space probes which have been operating for over 34 years and have now left the solar system.

So far we have made the assumption that the electrical and thermal properties of the n-type and p-type semiconductor legs are identical. This is seldom, if ever, the case in real thermoelectric materials. ZT needs to be redefined with the Seebeck coefficients, electrical

http://dx.doi.org/10.5772/57092

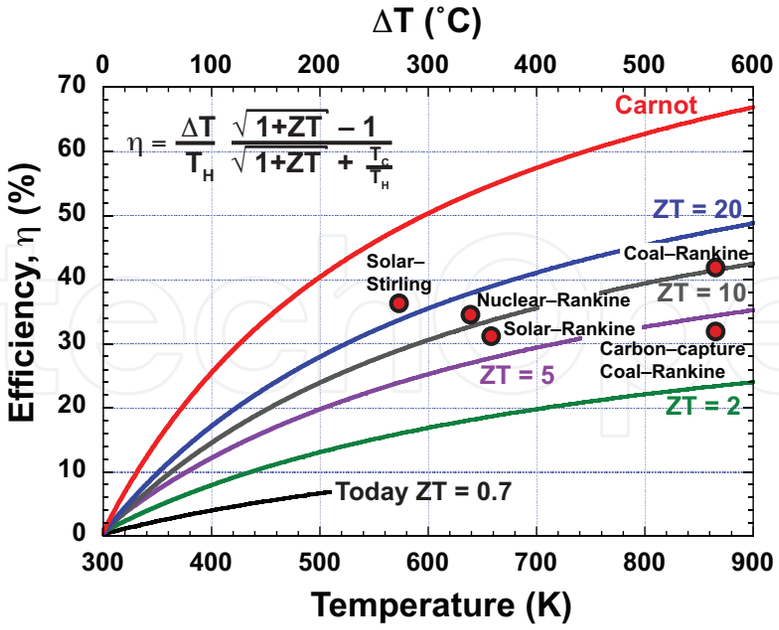

Figure 7. The thermodynamic efficiency of thermoelectric materials as a function of ZT assuming a cold side temperature of 298 K (25 ^{o}C). Also included is the Carnot efficiency and comparisons to Rankine and Stirling thermodynamic cycles.

conductivities and thermal conductivities defined for both n-type and p-type semiconductors to give

$$ZT = \frac{(\alpha_p - \alpha_n)^2 T}{\left[\sqrt{\frac{\kappa_p}{\sigma_p}} + \sqrt{\frac{\kappa_n}{\sigma_n}}\right]^2} \tag{32}$$

For n-type and p-type semiconductor legs of length (area), L_n (A_n) and L_p (A_p) respectively, ZT is a maximum value when the total resistance of the legs times the thermal conductance is a minimum value. This occurs when

$$\frac{L_n A_p}{L_p A_n} = \sqrt{\frac{\sigma_n \kappa_n}{\sigma_p \kappa_p}} \tag{33}$$

Up to this point we have assumed that we have a ΔT applied across each of the n- and p-type legs of the thermoelectric module. Since each leg has a given thermal conductivity, only a finite ΔT can be sustained across the thermoelectric legs. This therefore sets a maximum ΔT that can be sustained due to the thermal conductivity and in terms of ZT it is defined as

$$\Delta T_{max} = \frac{1}{2} Z T_c^2 \tag{34}$$

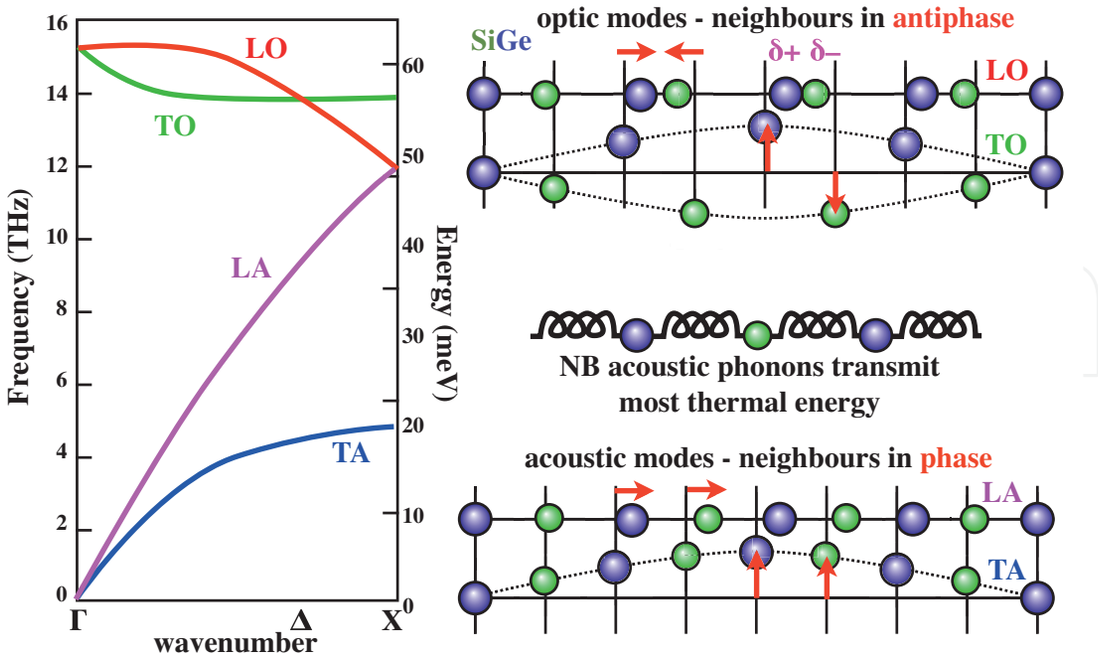

Figure 8. Left: The phonon energy dispersion versus wavenumber for Si. Right: schematic diagrams of the optic modes and acoustic modes in terms of the spring model for the lattice bonds between atoms in the crystal for an alloy of $Si_{0.5}Ge_{0.5}$.

4. Thermal conductivity

The thermal conductivity is one of the key parameters that many researchers aim to reduce to improve the ZT of a material. The thermal and electrical conductivities in bulk materials are linked as was first demonstrated by Wiedemann and Franz. They made the empirical observation that the thermal conductivity divided by the electrical conductivity times temperature was a constant for all metals. One of the greatest successes of the Drude theory of metals was the explanation of the Wiedemann-Franz law as it is now called. The Drude model assumes that the bulk of the thermal transport in metals is by the conduction electrons. This is now know to be incorrect and the success of the Drude model in explaining the Wiedemann-Franz law was a fortuitous cancelation of two factors of 100. It is now known that the Drude approach of applying the classical gas laws cannot be applied to electron gases in solids. The Wiedemann-Franz law, however, is still correct for degenerately doped bulk semiconductors and metals and provides substantial limitations when trying to optimize thermoelectric materials.

Quantum theory now provides a more complete description of the thermal conductivity which will be described. Phonons are the modes of vibrations of interacting particles in elastic crystal lattices. Phonons are quasi-particles which describe the collective excitations of the lattice (modes of vibrations). Fig. 8 shows the simple semi-classical interpretation where the bonds between atoms in a lattice are considered as springs and then by solving the Helmholtz wave equation for the vibrational modes of these springs throughout the lattice, the energy dispersion curves for the phonons can be calculated. Whilst more accurate description of the phonons requires much more detailed quantum mechanical calculations, this simple picture provides the same overall physical picture of the modes. There are two types of modes: optic and acoustic. The acoustic modes are where the oscillations

of neighbours are in phase either in a transverse or longitudinal direction whilst the optics modes have the neighbours oscillating in anti-phase and are therefore at higher energy.

The total thermal conductivity of a semiconductor or metal can be divided into the electrical contribution, κ_{el} and the lattice contribution from phonons, κ_{ph}, i.e.

$$\kappa = \kappa_{el} + \kappa_{ph} \tag{35}$$

For non-degenerate semiconductors (low carrier density), $\kappa_{el} \ll \kappa_{ph}$ whilst for degenerate semiconductors (high carrier densities including metals) , $\kappa_{el} \gg \kappa_{ph}$. An ideal thermoelectric material should have both high carrier density and a decoupling of the thermal conductivity with $\kappa_{el} \ll \kappa_{ph}$ but Wiedemann-Franz prevents this in bulk semiconductors and metals.

In metals where κ_{el} dominates the the thermal conductivity, Wiedemann-Franz produces

$$\frac{\sigma T}{\kappa} = \frac{3}{\pi^2}\left(\frac{q}{k_B}\right)^2 = \frac{1}{L} \tag{36}$$

where L is the Lorenz number which is equal to 2.44×10^{-8} WΩK^{-2}. There are a number of examples where the Wiedemann-Franz law breaks down which include pure metals at low temperature, alloys where the small κ_{el} from high electron scattering results in significant contributions from κ_{ph} and certain low dimensional structures where κ_{ph} can dominate over κ_{el}.

The lattice contribution is in quantum theory the phonon contribution to the thermal conductivity where phonons are the quantised vibration of the lattice. The phenomenological model using phonon scattering which is now used to calculate the phonon contribution to the thermal conductivity this that first published by Callaway [3]. It assumes that the phonon scattering processes can be represented by frequency-dependent relaxation times and uses a formula derived from the Boltzmann transport equation to calculate the thermal conductivity. The lattice thermal conductivity calculated by this approach is

$$\kappa_{ph} = \frac{k_B}{2\pi^2}\left(\frac{k_B}{\hbar}\right)^3 \int_0^{\frac{\theta_D}{T}} \frac{\tau_c(x)x^4e^x}{v(x)(e^x-1)^2}dx \tag{37}$$

where θ_D is the Debye temperature, $x = \frac{\hbar\omega}{k_B T}$, $\hbar$ is Planck's constant divided by 2π, ω is the phonon angular frequency, τ_c is the combined phonon scattering time and v is the phonon velocity. The integral has to include all the acoustic and optical phonon modes although there are particular types of systems where for example transport of optical phonons can be forbidden in small enough nanostructures.

The electrical contribution to the thermal conductivity was derived from the Boltzmann transport equation by Nag [4]. For total electron momentum relaxation times of τ for electrons of energy, E, the electron contribution to the thermal conductivity is

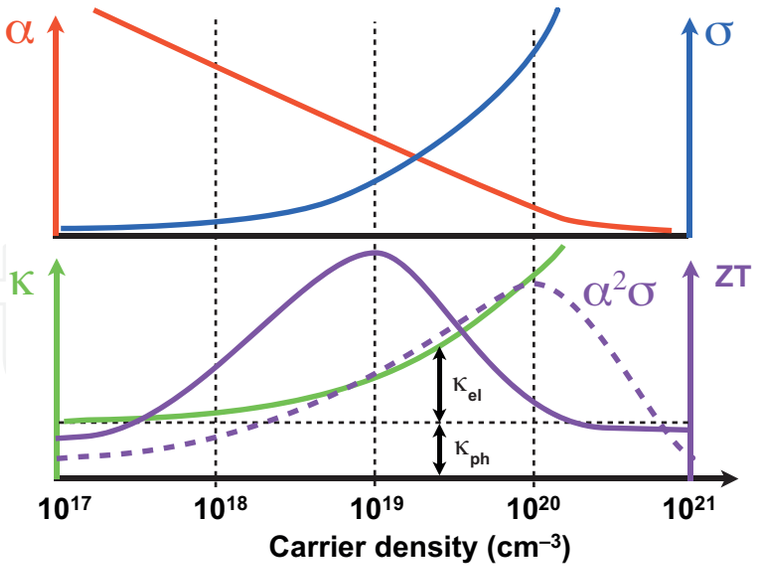

Figure 9. The ZT, Seebeck coefficient, electrical conductivity, thermal conductivity and power factor versus carrier density for a typical semiconductor.

$$\kappa_{el} = \frac{\sigma}{q^2 T}\left[\frac{\langle\tau\rangle\langle E^2\tau\rangle - \langle E\tau\rangle^2}{\langle\tau^3\rangle}\right] \tag{38}$$

The clear result that is not ideal for optimising thermoelectric materials at high carrier densities is that $\kappa_{el} \propto \sigma$.

5. Optimising ZT

In bulk semiconductor thermoelectric materials, once a material with a particular composition has been chosen, the only real parameter that can be varied to optimise ZT is the doping density. The electrical and thermal parameters in bulk materials are coupled through the Wiedemann-Franz law and so simply by improving one parameter through choosing a better doping does not necessarily result in higher ZT. Fig. 9 shows a schematic diagram of the electrical and thermal properties of the bulk thermoelectric semiconductor material Bi_2Te_3 as a function of doping density. For this example, the maximum ZT is close to 10^{19} cm^{-3} whilst the maximum power factor is at 10^{20} cm^{-3}. The figure also demonstrates the coupling of the electrical and thermal conductivities at high carrier densities and the inverse relationship between carrier density and the Seebeck coefficient ($\alpha \propto n^{-\frac{2}{3}}$ where n is the carrier density).

A comparison of the best n-type and p-type ZT values as a function of temperature is demonstrated in Fig. 10. The solid lines are the ZT values for bulk materials. The majority of the 3D bulk results all have ZT values that are around 1 or less. No bulk material has yet been found with a ZT significantly higher than 1. There have, however, been a number of suggestions to improve ZT by going to lower dimensional structures where the

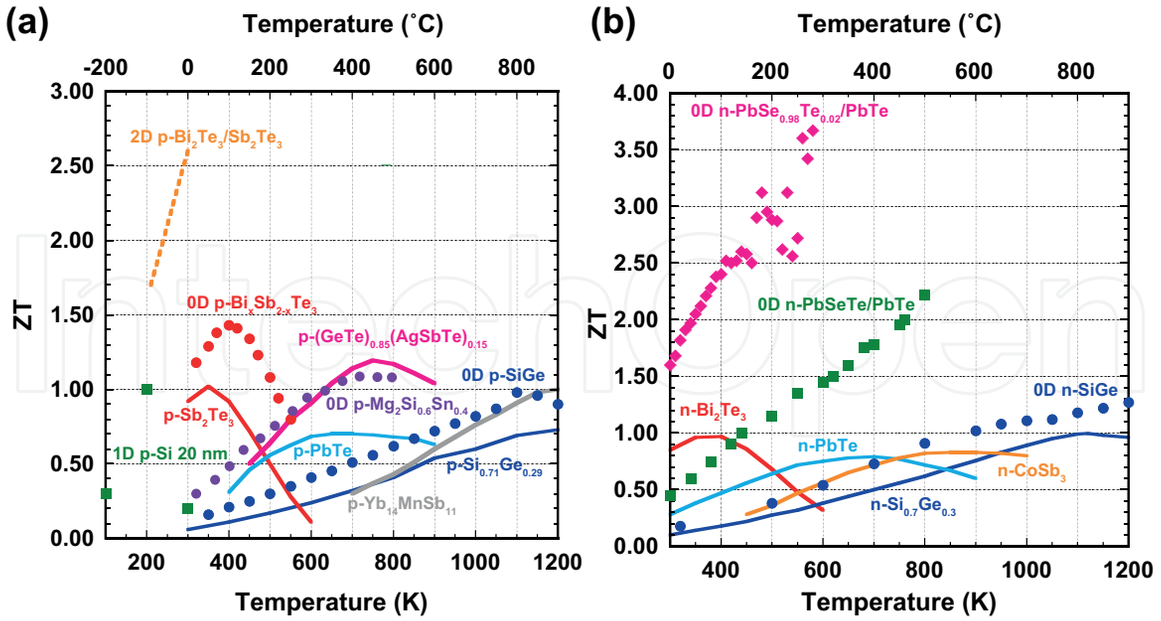

Figure 10. Left: a comparison of ZT for p-type material as a function of temperature (p-Sb_2Te_3, p-PbTe, p- $CeFe_4Sb_{12}$, p-$Yb_{14}MnSb_{11}$ [5], p-$Si_{0.71}Ge_{0.29}$ [6], 2D p-Bi_2Te_3/Sb_2Te_3 [7], 1D Si [8], 0D p-SiGe [9], p-$(GeTe)_{0.85}(AgSbTe)_{0.15}$ [10], 0D p-$Bi_xSb_{2-x}Te_3$ [11], 0D $Mg_2Si_{0.4}Sn_{0.6}$ [12]). Right: a comparison of ZT for n-type material as a function of temperature (n-Bi_2Te_3, n-PbTe, n-$CoSb_3$ [5], n-$Si_{0.7}Ge_{0.3}$ [6], 0D PbSeTe [13], 0D n-SiGe [14], 0D n-$PbSe_{0.98}Te_{0.02}$/PbTe [15]).

Wiedemann-Franz rule can break down and quantum effects can be used to optimise the ZT value which will be discussed in the next section.

The first major calculations to demonstrate the advantages of moving to low dimensional structures was that of Mildred Dresselhaus [16]. There are multiple ways that low dimensional structures can enhance the value of ZT.

5.1. Low dimensional structures

Before demonstrating the potential enhancements that low dimensional structures can bring to the ZT of a thermoelectric material, the definition of lower dimensional samples must be considered. If a sample is made with dimensions of length, L, width, w and thickness, t then the dimensionality of the system and the appropriate transport regime for electrons or phonons is inferred by comparing the sample dimension to the various scattering lengths and characteristics lengths defined below. Care is always required for a sample can be, for example, the 2D in terms of electrical transport but 3D in terms of thermal transport.

In the Drude model, the electrical conductivity is defined in terms of the elastic scattering time, τ, the effective mass of the electrons in the material, m^* and the carrier density, n as

$$\sigma = \frac{nq^2\tau}{m^*} \tag{39}$$

This equation is very simplistic in terms of the mechanisms which determine the electrical conductivity and dependent on the temperature and material, additional transport

and scattering mechanisms including disorder, electron-electron interactions, quantum interference or ballistic transport have to be included. Generally the length scale, l_x associated with a scattering time, τ_x for some scattering process is linked through the diffusion constant, D as

$$l_x = \sqrt{D\tau_x} \tag{40}$$

In this form the mobility is defined as $\mu = \frac{q}{m^*}\tau$ and the Einstein relation relates the mobility to the diffusion constant for an absolute temperature, T as

$$\mu = \frac{qD}{k_B T} \tag{41}$$

In most electronic conduction it is only the electrons close to the Fermi level in energy that need to be considered for which the relevant scale is the Fermi wavelength

$$\lambda_F = \frac{2\pi}{k_F} = \sqrt{\frac{2\pi}{n}} = \frac{h}{\sqrt{2m^* E_F}} \tag{42}$$

The elastic scattering length of electrons is defined as the mean free path, ℓ. (Note - the mean free path is strictly defined as the shortest scattering length between all the scattering mechanisms which includes phase coherent scattering, inelastic scattering, electron-electron scattering, but normally the elastic scattering length is the dominant.) The mean free path is defined generally and for lower dimensions as

$$\ell = v_F \tau = \frac{\hbar k_F}{m^*}\tau \tag{43}$$

$$\ell_{3D} = \frac{\hbar}{m^*}(3\pi^2 \frac{n}{g_v})^{\frac{1}{3}} \frac{\mu m^*}{q} = \frac{\hbar\mu}{q}(3\pi^2 \frac{n}{g_v})^{\frac{1}{3}} \tag{44}$$

$$\ell_{2D} = \frac{\hbar\mu}{q}\sqrt{2\pi \frac{n}{g_v}} \tag{45}$$

$$\ell_{1D} = \frac{\hbar\mu}{q}\pi \frac{n}{g_v} \tag{46}$$

where g_v is the valley degeneracy of the semiconductor. The above equations have assumed that the electrons have a spin degeneracy of 2 which is only untrue under large magnetic fields sufficiently high to split the spin degeneracy.

Moving to thermal transport there are a number of models which can be considered to determine the appropriate length scales. The first is the thermal length, L_T defined as the

length over which thermal smearing and the associated phase randomization of an electron of the Fermi distribution which produces and energy uncertainty of $k_B T$. This is given by

$$L_T = \sqrt{\frac{D\hbar}{k_B T}} \tag{47}$$

The phonon group velocity is defined as $\frac{\partial \omega}{\partial q}$ where ω is the phonon angular frequency and q is the phonon wavenumber. The phonon mean free path in the 3D bulk as determined by the Debye theory, which assumes that the phase and group velocity of the phonons are equal, is give by

$$\Lambda_{ph} = \frac{3\kappa_{ph}}{C_v \langle v \rangle \rho} \tag{48}$$

where C_v is the specific heat capacity at constant volume, $\langle v \rangle$ is the average phonon velocity and ρ is the density of phonons. Table **??** gives examples of the phonon mean free path in Si and germanium. The Debye theory is by no means unique and the group velocity of phonons is defined in terms of the phonon dispersion relation as demonstrated by Chen [17]. Table **??** provides a comparison between the mean free paths determined by the Debye and dispersion models. There is a significant difference between the two approaches and this is one of the main issues and problems in determining exactly which dimensionality a system is in terms of the thermal transport. In all the 3D cases below, the numbers are larger than the equivalent electron mean free path.

Material	Model	Specific heat ($\times 10^6$ Jm^{-3}K^{-1})	Group velocity (m s^{-1})	Phonon mean free Λ_{ph} (nm)	Debye temperature (K)
Si	Debye	1.66	6400	40.9	645
Si	Dispersion	0.93	1804	260.4	645
Ge	Debye	1.67	3900	27.5	360
Ge	Dispersion	0.87	1042	198.6	360

Table 1

5.2. Quantum wells

Before describing how low dimensional systems can improve ZT, we first require to find the energy solutions for a low dimensional systems. The simplest solution to investigate is the 2D quantum well for electrons, (Fig. 11) where the approximation is made that the potential energy for electrons inside the quantum, V = 0 and the potential energy outside the well is infinite ($V = \infty$). We require to solve the time independent Schrödinger equation which is

$$-\frac{\hbar^2}{2m^*}\frac{\mathrm{d}^2\psi(z)}{\mathrm{d}z^2} + V(z)\psi(x) = E\psi(z) \tag{49}$$

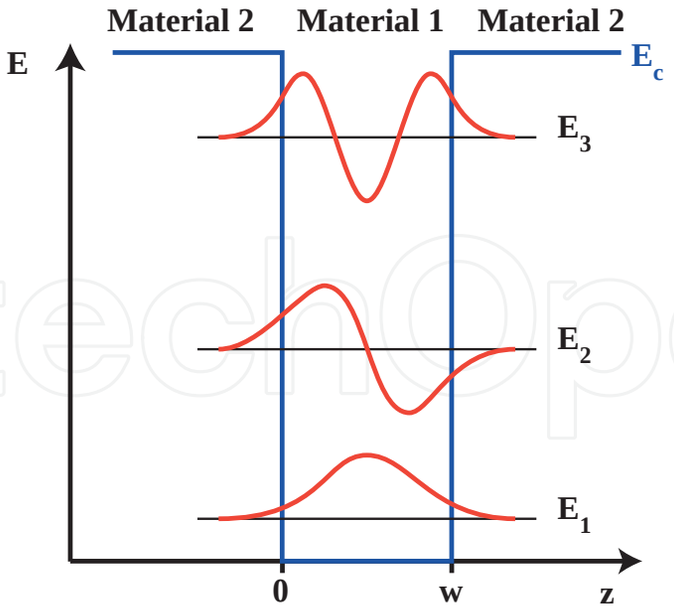

Figure 11. The quantized energy states in a quantum well of width, w.

Outside the quantum well with $V = \infty$, there are no solutions and the electrons are forbidden to occupy regions outside the quantum well. Inside the quantum well $V(z) = 0$ and so the Schrödinger equation reduces to the Helmholtz or wave equation

$$-\frac{\hbar^2}{2m^*}\frac{\mathrm{d}^2\psi(z)}{\mathrm{d}z^2} = E\psi(z) \tag{50}$$

Any travelling wave solution is a valid solution inside the quantum well to this equation so $\psi(z) = A\sin(kz)$, $\psi(x) = A\cos(kz)$, $\psi(z) = Ae^{ikz}$ and $\psi(x) = Ae^{-ikz}$ (where A is an amplitude of the wavefunction) and any mixture of these equations are all potential valid trial solutions. The boundary conditions that a solution must adhere to is that at $z \to \infty$ then $\psi(\pm\infty) = 0$. For the infinite quantum well in Fig. 11 this requires $\psi(0) = \psi(w) = 0$ and so the wavefunctions cannot penetrate outside the quantum well. Also $\psi(z)$ and $\frac{\mathrm{d}\psi}{\mathrm{d}z}$ must be continuous between regions. These boundary conditions therefore require that the only possible solution is

$$\psi(z) = A_n\sin(k_n z) \quad \text{with } k_n = \frac{n\pi}{w} \text{ and } n = 1, 2, 3, \ldots \tag{51}$$

If this wavefunction is substituted back into the Schrödinger equation then the solution for the energy is

$$E = \frac{\hbar^2 k_n^2}{2m^*} = \frac{\hbar^2\pi^2 n^2}{2m^* w^2} \text{ for } n = 1, 2, 3, \ldots \tag{52}$$

http://dx.doi.org/10.5772/57092

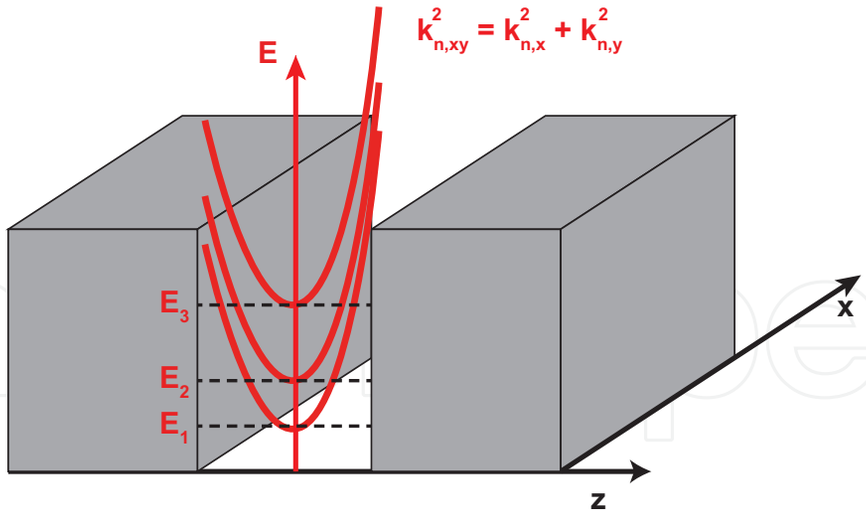

Figure 12. The quantized energy states in a quantum well of width, w.

The integers $n = 1, 2, 3, \ldots$ are called quantum numbers and the solutions provide quantized energy levels that restrict the energy of the electrons into subband states indicated by E_1, $E_2, \ldots E_n$. Whilst in any classical system that has a continuous range of energies the ground state can always have zero energy, in this quantized system however, the ground state with $n = 1$ always has energy. This is known as the zero point energy. In semiconductor materials, if two different materials are placed together then a heterostructure results. By placing one material with a lower conduction band between the same material with a higher conduction band, a quantum well is produced as shown in Fig. 11. The electrons move along the x- and y-directions of the quantum well and are quantized in the z-direction then the electrons have parabolic energy dispersions along the x- and y-directions and the quantized energy dispersion only along the z-direction as shown in Fig. 12. This results in the complete energy of each electron subband to be

$$E = \frac{\hbar^2 k_x^2}{2m^*} + \frac{\hbar^2 k_y^2}{2m^*} + \frac{\hbar^2 \pi^2 n^2}{2m^* w^2} \quad \text{for} \quad n = 1, 2, 3, \ldots \tag{53}$$

5.3. Density of states

Equations 6 and 8 both use the density of states, $g(E)$ which describes the number of available states that electrons can occupy in any material system. The density of states is defined as the number of states per energy per unit volume of real space where if N is the number of states then

$$g(E) = \frac{\mathrm{d}N}{\mathrm{d}E} \tag{54}$$

The density of states is therefore counting the number of states between E and $E + \mathrm{d}E$ in energy. In **k**-space, the total number of states, N is equal to the volume of the sphere or

radius **k** first divided by volume occupied by one state and then divided by the volume of real space. Therefore if we have a 3D volume defined by a cube with side length, L then the volume of one state in **k**-space is $\left(\frac{2\pi}{L}\right)^3$. The number of states is given by

$$N = g_v g_s \frac{4\pi k^3}{3} \frac{1}{\left(\frac{2\pi}{L}\right)^3} \frac{1}{L^3} \tag{55}$$

$$= g_v g_s \frac{4\pi k^3}{3\left(2\pi\right)^3} \tag{56}$$

where the degeneracy of valleys, g_v and the spin degeneracy g_s have been added. For direct bandgap semiconductors, $g_v = 1$ whilst for indirect bandgap semiconductors the valley degeneracy will be greater than 1. As an example, g_v = 2 for silicon. The spin degeneracy, g_s is virtually always 2 for the majority of systems and this only changes for systems with strong magnetic fields. The trick to working out the density of states is to split the derivative in equation 54 into

$$g(E) = \frac{\mathrm{d}N}{\mathrm{d}E} = \frac{\mathrm{d}N}{\mathrm{d}k}\frac{\mathrm{d}k}{\mathrm{d}E} \tag{57}$$

so that equation 56 becomes

$$\frac{\mathrm{d}N}{\mathrm{d}k} = g_v g_s \frac{4\pi k^2}{\left(2\pi\right)^3} \tag{58}$$

The parabolic bands of the effective mass theory provide $E = \frac{\hbar^2 k^2}{2m^*}$ which rearranging gives

$$k = \sqrt{\frac{2m^* E}{\hbar^2}} \tag{59}$$

Taking the derivative with respect to energy produces

$$\frac{\mathrm{d}k}{\mathrm{d}E} = \sqrt{\frac{2m^*}{\hbar^2}} \frac{E^{-\frac{1}{2}}}{2} \tag{60}$$

Equations 58 and 60 can now be combined to produce the 3D density of states

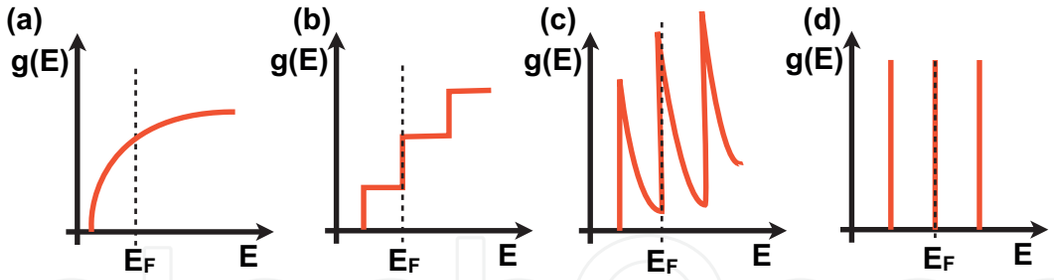

Figure 13. The electron density of states as a function of energy for (a) 3D (b) 2D (c) 1D and (d) 0D semiconductor systems.

$$g_{3D}(E) = \frac{g_v g_s}{4\pi^2}\left(\frac{2m^*}{\hbar^2}\right)^{\frac{3}{2}} E^{\frac{1}{2}} \tag{61}$$

The same technique can be repeated for 2D systems where instead of a sphere, the 2D

equivalent is a circle in **k**-space. Repeating the technique for the 3D system, the number of states is

$$N_{2D} = g_v g_s \frac{\pi k^2}{3}\frac{1}{\left(\frac{2\pi}{L}\right)^2}\frac{1}{L^2} \tag{62}$$

$$= g_v g_s \frac{\pi k^2}{(2\pi)^2} \tag{63}$$

and repeating the techniques above results in the 2D density of states as

$$g_{2D}(E) = g_v g_s \frac{m^*}{2\pi\hbar^2} \tag{64}$$

This results is for a single subband in a quantum well (see Figs. 11 and 12) and for a heavily doped system as most thermoelectric materials are requires a summation of the density of states over all the subbands. This results in the 2D density of states at an energy, E being the sum over all subband below that energy which is

$$g_{2D}(E) = \sum_{i=1}^{n} g_v g_s \frac{m^*}{2\pi\hbar^2}\Theta(E - E_i) \tag{65}$$

where Θ is the Heaviside step function.

The technique can be repeated for 1D and 0D systems and to summarise the density of states as a function of dimension are

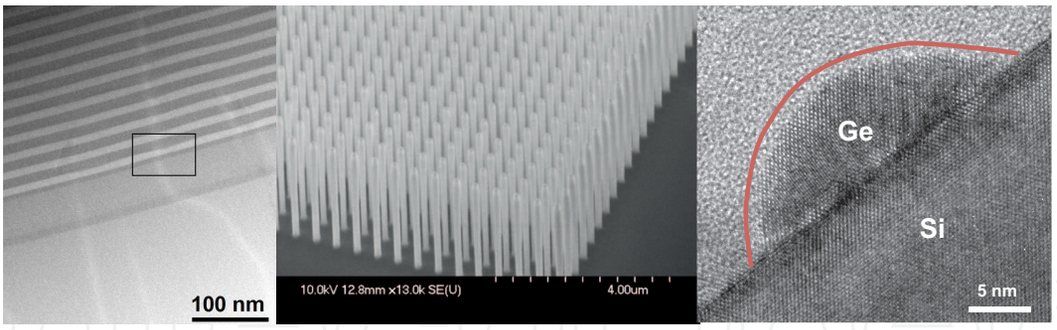

Figure 14. Left: A cross sectional TEM image of Ge quantum wells with $Si_{0.2}Ge_{0.8}$ barriers forming a 2D thermoelectric system [18]. The square highlights a dislocation that limits the performance of this material. Middle: A SEM image of etched 50 nm wide nanowires of Ge/$Si_{0.2}Ge_{0.8}$ material forming 1D thermoelectric systems. Right: A TEM image of a Ge quantum dot grown on a silicon substrate forming a 0D thermoelectric system for scattering phonons.

$$g_{3D}(E) = \frac{g_v g_s}{4\pi^2}\left(\frac{2m^*}{\hbar^2}\right)^{\frac{3}{2}} E^{\frac{1}{2}} \tag{66}$$

$$g_{2D}(E) = \sum_{i=1}^{n} g_v g_s \frac{m^*}{2\pi\hbar^2}\Theta\left(E - E_i\right) \tag{67}$$

$$g_{1D}(E) = \frac{1}{2\pi\hbar}\sum_{i=1}^{n} g_v g_s \sqrt{\frac{m^*}{2}}\pi\hbar^2\Theta\left(E - E_i\right) \tag{68}$$

$$g_{0D}(E) = \sum_{i=1}^{n} g_v g_s \delta\left(E - E_i\right) \tag{69}$$

with $\delta(E - E_i)$ the Dirac delta function.

5.4. Low dimensional enhancements to ZT

The density of states as a function of energy for 3D, 2D, 1D and 0D are plotted in Fig. 13. Also plotted is the ideal position for the Fermi energy if the Seebeck coefficient is to be maximised using the Cutler and Mott equation

$$\alpha = -\frac{\pi^2}{3q}k_B^2 T\left[\frac{d\ln(\mu(E)g(E))}{dE}\right]\Bigg|_{E=E_F} \tag{70}$$

By moving to lower dimensional structures, there is a larger asymmetry in the density of states around the Fermi energy and the above equation and the discussions in section 2 indicates that this increases the Seebeck coefficient. Therefore by choosing systems with lower dimensions, the Seebeck coefficient can be enhanced. A number of experimental examples have demonstrated significant improvements to the Seebeck coefficient from reducing the dimensionality from 3D to 2D, 1D or 0D. Examples of the physical structures are shown in Fig. 14. Quantum wells with the transport either parallel or perpendicular to

the quantum wells are used for 2D thermoelectric systems (see Fig. 14 left). Nanowires either grown or etched can be used to form 1D thermoelectric systems (Fig. 14 middle) whilst most 0D thermoelectric systems use quantum dots that are aimed at scattering phonons (Fig. 14 right).

2D quantum well systems can also enhance the electrical conductivity by a number of techniques. If the electrical and thermal transport is along quantum wells then modulation doping can be used to enhance the electrical conductivity. Here the dopants are only placed in the barriers which are at higher energy than the quantum well. The carriers fall into the quantum well and are therefore remote from the ionised dopants that created the carriers. By separating the carriers from the dopants, the Coulomb scattering is reduced and the mobility and electrical conductivity increases. This occurs along with the Seebeck enhancement described above and so higher power factors can be created. The potential disadvantage of this technique is that the electrical conductivity can be so large that it also can increase the thermal conductivity in a detrimental way to the ZT. By optimising the parameters, higher ZTs can be produced.

The third approach to optimising ZT is to reduce the thermal conductivity. There are many ways to reduce the thermal conductivity by adding scattering centres or rough interfaces that scatter phonons. The main issue is to aim for a scattering technique that scatters phonons more than electrons. This is not as easy as it sounds. Adding 0D nanoparticles or quantum dots into a material has been successful at reducing κ faster than σ as shown in Fig. 10 in a number of material systems for both n- and p-type semiconductors [13, 15]. The quantum dots when of the correct size can scatter phonons much more easily than electrons especially for highly doped samples where the electron mean free paths are typically longer than phonon mean free paths. There are a number of examples of materials such as skutterudites where heavy atoms are inserted to fill voids in the lattice to have a similar effect at the microscale of the lattice [5].

2D superlattices with the electron transport perpendicular to the quantum well and barriers are also good at scattering phonons. The disadvantage of this type of superlattice is that the electrons or holes must quantum mechanically tunnel through the barriers which also significantly reduces the electrical conductivity to typically 3 to 4 times lower than bulk material. The lower thermal conductivity combined with the higher Seebeck from the 2D quantum wells does produce significant enhancements to ZT as show in Fig. 10 [7].

Finally 1D nanowires have also demonstrated substantial improvements to ZT. Boukai et al., [8] demonstrated 10 nm wide Si nanowires which demonstrate enhanced Seebeck coefficients and significantly reduced thermal conductivities compared to bulk Si. The thermal conductivity demonstrated the largest changes with reductions of up to 150 times that of bulk silicon whilst the Seebeck improves by a factor of 2. ZTs at room temperature of 0.3 have been achieved with higher values at lower temperatures. The nanowires demonstrate how confining phonons in low dimensional structures can make significant changes to the ZT of a material.

6. The power output from thermoelectric modules

To this point the majority of this review has concentrated on ways to optimise ZT but for applications it is the current and voltage i.e. the output power produced that is the most

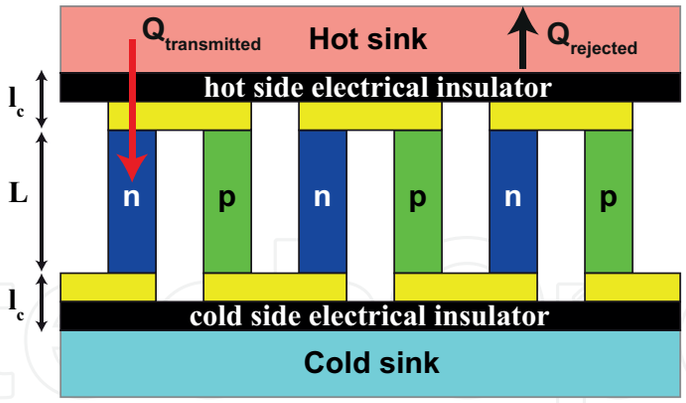

Figure 15. A schematic diagram of a complete module with leg length, L and contact length, l_c.

important parameter for applications. Therefore it is important to understand the issues of the output power and how it may be optimised. We will start by considering a complete module as shown in Fig. 15. As the Seebeck coefficient of most materials is $\ll 1$ mV/K and most applications will require at least 1 V and in many cases multiple Volts, a large number of legs must be connected in series to achieve suitable output voltage for the applications. If we have N legs each of length, L, with thermal conductivity, κ and contacts of length, l_c with thermal conductivity, κ_c then the voltage produced is given by [19]

$$V = \frac{\alpha N \Delta T}{1 + 2\frac{\kappa l_c}{\kappa_c L}} \tag{71}$$

The current can also be calculated and for legs of area A and electrical conductivity, σ with specific contact resistivity, ρ_c, the current is

$$I = \frac{\alpha \sigma A \Delta T}{2(\rho_c \sigma + L)(1 + 2\frac{\kappa l_c}{\kappa_c L})} \tag{72}$$

By multiplying the voltage and current together, the resulting power is

$$P = \frac{\alpha^2 \sigma A N \Delta T^2}{2(\rho_c \sigma + L)(1 + 2\frac{\kappa l_c}{\kappa_c L})^2} \tag{73}$$

There are a number of issues that the power equation highlights. The first is that the power is dominated by $\alpha^2\sigma$ which is called the power factor. The second is that the power is proportional to the area of the legs and the number of the legs in the module. The power is also proportional to the square of ΔT. Finally, whilst shortening the length of the legs in the module to first order will increase the power, equation 73 demonstrates that as the leg length reduces, the contact resistance of each leg plays a larger part in reducing the output power. For the microfabricated modules, having a low specific contact resistivity can be as important as a material with high ZT and power factor in being able to achieve a high output power.

http://dx.doi.org/10.5772/57092

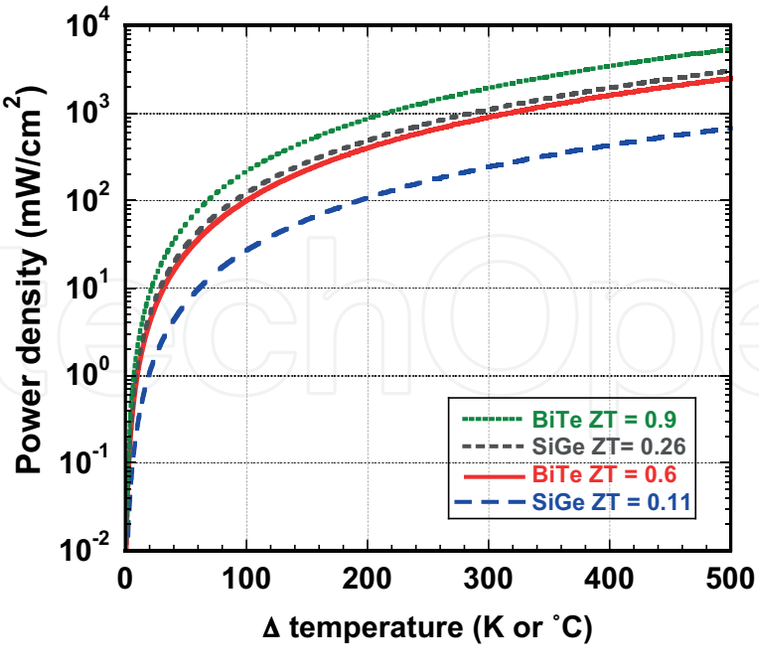

Figure 16. The power as calculated from equation 73 for a module with 525 legs of area 500 μm $\times$ 50 μm, leg length of L = 20 μm and l_c = 10 nm.

Another issue is that for many applications the amount of heat may vary and is not constant. Therefore power conditioning along with electrical impedance matching is required so that the thermoelectric module can always operate at the maximum power point. Maximum power point tracking systems are required which automatically adjust the load impedance so that it is always matched to the thermoelectric for all levels of heat and ΔT being applied across the thermoelectric.

Material Units	$\alpha_p - \alpha_n$ (μV/K)	σ (S/m)	κ (W/mK)	ZT @ 300 K	ρ_c Ω-cm^2
BiTe	500	71468	2	0.67	10^{-7}
BiTe	500	71468	2	0.67	10^{-7}
SiGe	600	70000	7.3	0.26	10^{-8}
SiGe	500	27900	4.8	0.22	10^{-8}

Table 2

7. Applications

The first thermoelectric application was to power satellites for space applications in 1961 [20]. Space systems use radioisotope thermoelectric generators (RTGs) where a radioactive material heated by the decay and emission of radiation is used as the hot source with a thermoelectric generator to turn the heat into electricity. Plutonium 238 was the main power source used by NASA in most of their 28 RTG systems which operates with temperatures up to 1000 ^{o}C whilst the outside of the spacecraft is used with heat exchangers to provide the cold sink. With such high temperatures, SiGe has been the main thermoelectric material

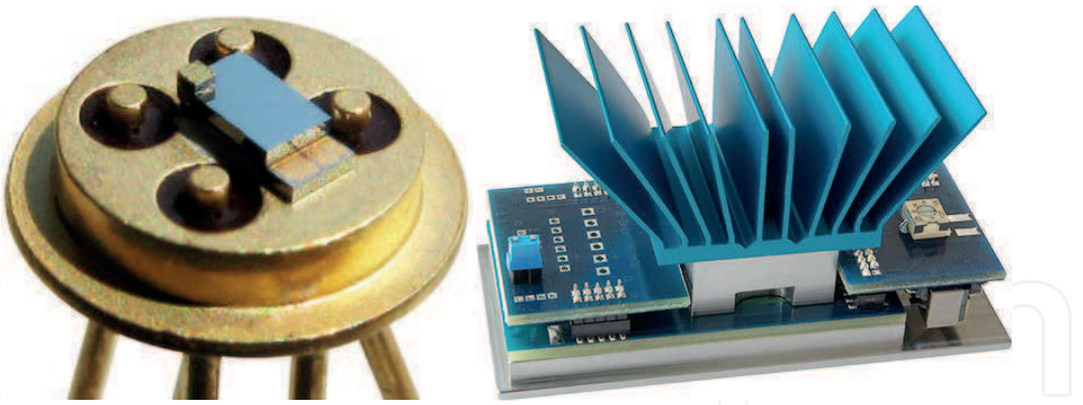

Figure 17. Left: a telecoms laser on a microfabricated Peltier cooler produced by Micropelt. Right: a thermoelectric generator produced by Micropelt showing the cold sink aimed at dissipating heat through air cooling. Copyright Micropelt [21].

used for these generators and the efficiencies can be as high as 6.6 % mainly due to the high ΔT. Both Voyager space missions which are now outside the solar system are powered by SiGe RTGs weighing 37.7 kg and provided 470 W on launch at 40 V. Over a period of time the temperature of the plutonium reduces as a function of the half-life of the radioactive decay so the systems are now generating less than 350 W, 34 years after launch. This is one of the best demonstrations of the robustness of the thermoelectric generator as for such space systems now over a light year away from earth, the power sources must be fit and forget. One problem is that there are no present sources of plutonium 238 as all the weapons nuclear reactors have been shut down and so there are a number of research programmes aiming to develop new RTG technology using available radio isotopes.

The major application for thermoelectric devices at present is as Peltier coolers (Fig. 17 left) to maintain a low temperature for electronic and optoelectronic components such as telecoms lasers and rf sources. It is therefore in the use as a cooler rather than generating electricity that thermoelectrics are predominantly used at present. A number of companies are offering thermoelectric generator demonstrator kits as products (Fig. 17 right) to allow companies to test thermoelectrics for specific applications. The major present applications are for generating electricity to run sensors in a range of predominantly industrial environments where ΔTs between 20 and 100 ^{o}C can provide sufficient energy for the sensors. The majority of the energy use in the sensors is for the wireless communication that for mobile phone system communication will require powers around 5 mW while many of the sensing elements only require sub-μW powers for making a measurement. These wireless industrial sensing applications are widespread and the cost of the thermoelectric device becomes economical for systems where no installation of wires for communication and/or long term power. It is the large cost of replacing batteries (mainly labour costs) that allows thermoelectrics and other forms of energy harvesting to be cost effect. Most wireless sensors systems now require between 1 and 5 mW of power to run mainly dependent on the distance for the communication and so a square cm area thermoelectric device requires around 50 ^{o}C to provide sufficient power. As the communications consumes the most power, most systems have rechargable battery or super-capacitor storage systems and then use burst modes of communication so that information is only sent when required to save power.

Research results have been published on clothing with integrated thermoelectrics [22]. Only small ΔTs can be provided across clothing using the air temperature outside the

http://dx.doi.org/10.5772/57092

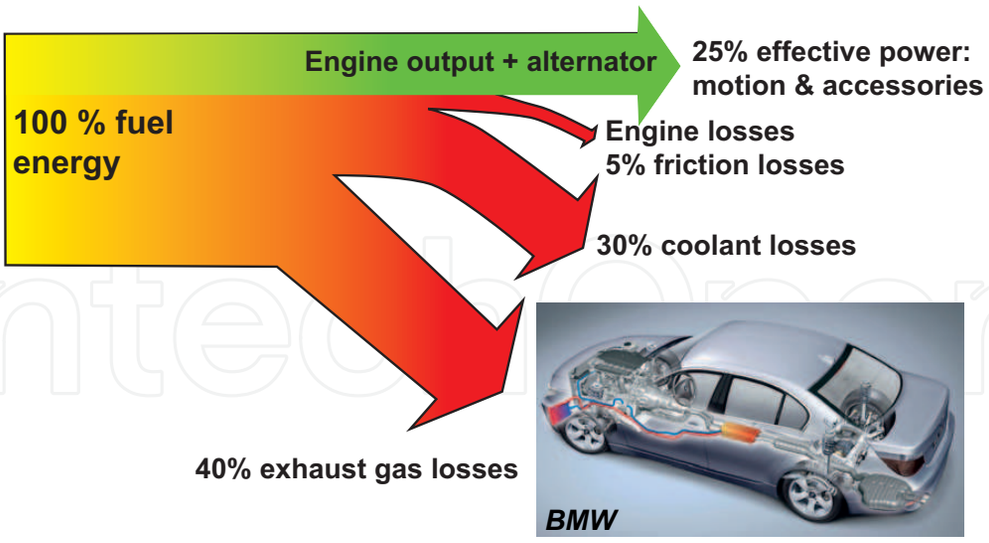

Figure 18. A schematic diagram of how the energy from a combustion engine in a car is distributed. 25% of the energy produces motion and through the alternator generates electricity to power accessories including the electrics, the air conditioning and the hifi system. 75% of the energy from the fuel is lost mostly through friction and heat. 40% of the fuel energy disappears through the exhaust system hence there is interest in using thermoelectrics to harvest some of this waste energy.

body to provide the cold side temperature. There is enormous interest in such power sources for autonomous wireless health monitoring systems that can be fit and forget. Electrocardiography systems integrated into the clothing and powered by thermoelectrics have already been demonstrated and even tested through cycles of washing in washing machines to check the robustness of the technology. For this technology to be practical, batteries or super capacitors and power management must also be integrated along with the sensors, some processing and communication technology. Whilst the low powers available with the small ΔTs may struggle to power the present communication systems, new short range communication protocols being developed at present for autonomous sensors by the IEEE are required before this type of application can be aggressively pursued.

The major driver for improved thermoelectrics at present is probably the car industry where European legislation to improve fuel efficiency is driving thermoelectrics research to replace the alternator. The car is an excellent system where thermoelectrics could play a big role as 75% of the fuel ends up as waste heat and the 40 % of waste heat that goes down the exhaust pipe into an environment that could be used to capture this heat and convert it into electricity (Fig. 18) [23, 24]. The temperature of the exhaust system can range from room temperature up to 750 ^{o}C so this is driving work on new thermoelectric materials to replace the best at present which is PbTe with toxic Pb that cannot be used for applications. Initial modelling has suggested that up to a 5% in fuel consumption could be achieved with suitable thermoelectrics with ZT of 1 but the key issue is getting the whole thermoelectric system cheap enough for the market. Also no thermoelectric provides ZT of 1 from room temperature to 750 ^{o}C so segmented modules and/or new materials are required. Most of the major car companies are now working heavily of thermoelectrics and it is only a mater of time before automotive systems become available.

A developing application is thermal photovoltaics. Concentrator photovoltaics are now producing efficiencies of around 45 % when the light is concentrated up to a thousand

times. These systems are aimed at solar farms which in sunny regions of the earth have the potential to produce power stations at the 100s of MW scale. Such concentration, however, results in the photovoltaic cells being heating to very high temperatures that results in large thermal cycling which ultimately produces failures reducing the lifetime of the systems. By integrating a thermoelectric with the photovoltaic, not only can electricity be generated from the heat thereby providing a joint and therefore improved system efficiency closer to the Carnot limit but more importantly, the thermoelectric cools the photovoltaic reducing the thermal cycling extremes and increases the lifetime of the system. This increase in lifetime results in substantially cheaper cost per Watt which is the major driver for photovoltaics. It is clear this will be a developing application for thermoelectrics in the future.

At present thermoelectrics requires a "killer application" before volume manufacture will result in widespread use. The automotive applications at present appear to be the major application driver, more by legislation rather than market but it is clear that the potential requirements for thermoelectric generators will improve as fossil fuel prices increase in the future. The autonomous sensor market may well also drive thermoelectrics but the real problem that must be solved is to find sustainable thermoelectric materials. Tellurium is the 9^{th} rarest element on earth predicted to run out before 2020 with the present use and so a key requirement for future thermoelectrics is that Te-free materials can be found that can be cheaply produced and with a high ZT and power factor. There is presently an enormous amount of research in thermoelectrics especially aiming to find Te-free materials and to produce modules for higher temperature applications such as the automotive energy harvesting. For students starting in a research career, this is one research area that is likely to expand over the next decades.

Author details

Douglas Paul

University of Glasgow, School of Engineering, Rankine Building, U.K.

References

[1] J.M. Ziman. *Electrons and Phonons*. Qxford University Press, 1960.

[2] Melvin Cutler and N. F. Mott. Observation of anderson localization in an electron gas. *Phys. Rev.*, 181(3):1336–1340, May 1969.

[3] J. Callaway. Model for lattice thermal conductivity at low temperatures. *Phys. Rev.*, 113(4):1046 – 1051, 1959.

[4] B.R. Nag. *Electron Transport in Compound Semiconductors*, volume 11 of *Solid State Sciences*. Springer, 1980.

[5] G. J. Snyder and E. S. Toberer. Complex thermoelectric materials. *Nature Materials*, 7(2):105–114, 2008.

[6] J.P. Dismukes, E. Ekstrom, D.S. Beers, E.F. Steigmeier, and I. Kudman. Thermal + electrical properties of heavily doped ge-si alloys up to 1300 degrees k. *J. Appl. Phys.*, 35(10):2899, 1964.

[7] R. Venkatasubramanian, E. Siivola, T. Colpitts, and B. O'Quinn. Thin-film thermoelectric devices with high room-temperature figures of merit. *Nature*, 413(6856):597–602, 2001.

[8] A. I. Boukai, Y. Bunimovich, J. Tahir-Kheli, J. K. Yu, W. A. Goddard, and J. R. Heath. Silicon nanowires as efficient thermoelectric materials. *Nature*, 451(7175):168–171, 2008.

[9] G. Joshi, H. Lee, Y. C. Lan, X. W. Wang, G. H. Zhu, D. Z. Wang, R. W. Gould, D. C. Cuff, M. Y. Tang, M. S. Dresselhaus, G. Chen, and Z. F. Ren. Enhanced thermoelectric figure-of-merit in nanostructured p-type silicon germanium bulk alloys. *Nano Letters*, 8(12):4670–4674, Dec 2008.

[10] D.M. Rowe, editor. *Thermoelectrics Handbook: Micro to Nano*, Boca Raton, FL, USA, 2006. CRC Press, Taylor and Francis.

[11] Yi Ma, Qing Hao, Bed Poudel, Yucheng Lan, Bo Yu, Dezhi Wang, Gang Chen, and Zhifeng Ren. Enhanced thermoelectric figure-of-merit in p-type nanostructured bismuth antimony tellurium alloys made from elemental chunks. *Nano Letters*, 8(8):2580–2584, 2008. PMID: 18624384.

[12] Q. Zhang, J. He, T. J. Zhu, S. N. Zhang, X. B. Zhao, and T. M. Tritt. High figures of merit and natural nanostructures in mg[sub 2]si[sub 0.4]sn[sub 0.6] based thermoelectric materials. *Applied Physics Letters*, 93(10):102109, 2008.

[13] T. C. Harman, P. J. Taylor, M. P. Walsh, and B. E. LaForge. Quantum dot superlattice thermoelectric materials and devices. *Science*, 297(5590):2229–2232, Sep 2002.

[14] X. W. Wang, H. Lee, Y. C. Lan, G. H. Zhu, G. Joshi, D. Z. Wang, J. Yang, A. J. Muto, M. Y. Tang, J. Klatsky, S. Song, M. S. Dresselhaus, G. Chen, and Z. F. Ren. Enhanced thermoelectric figure of merit in nanostructured n-type silicon germanium bulk alloy. *Appl. Phys. Lett.*, 93(19):193121, Nov 2008.

[15] T.C. Harman, M.P. Walsh, B.E. laforge, and G.W. Turner. Nanostructured thermoelectric materials. *J. Electronic Materials*, 34:L19–L22, 2005.

[16] L. D. Hicks and M. S. Dresselhaus. Effect of quantum-well structures on the thermoelectric figure of merit. *Phys. Rev. B*, 47(19):12727–12731, 1993.

[17] G. Chen. Thermal conductivity and ballistic-phonon transport in the cross-plane direction of superlattices. *Phys. Rev. B*, 57(23):14958–14973, Jun 1998.

[18] A. Samarelli, L.Ferre Llin, S. Cecchi, J. Frigerio, T. Etzelstorfer, E.Müller Gubler, Y. Zhang, J. R. Watling, D. Chrastina, G. Isella, J. P. Hague, J. Stangl, J.M.R. Weaver, P. S. Dobson, and D.J. Paul. The thermoelectric properties of ge/sige modulation doped superlattices. *J. Appl. Phys.*, 113:233704, 2013.

[19] D.W. Rowe and G. Min. Design theory of thermoelectric modules for electrical power generation. *Science, Measurement and Technology, IEE Proceedings -*, 143(6):351–356, 1996.

[20] R.D Abelson. Space missions and applications. In D.M. Rowe, editor, *Thermoelectric Handbook: Macro to Nano*, chapter 56, pages 56–1 – 56–29. Taylor and Francis, 2006.

[21] 2013.

[22] Vladimir Leonov, Tom Torfs, Chris Van Hoof, and Ruud J. M. Vullers. Smart wireless sensors integrated in clothing: an electrocardiography system in a shirt powered using human body heat. *Sensors & Transducers*, 107(8):165 – 176, 2009.

[23] K Matsubara and M Matsuura. A thermoelectric application to vehicles. In D.M. Rowe, editor, *Thermoelectric Handbook: Macro to Nano*, chapter 52, pages 52–1 – 52–11. Taylor and Francis, 2006.

[24] Jihui Yang and Francis R. Stabler. Automotive applications of thermoelectric materials. *Journal of Electronic Materials*, 38(7):1245 – 1251, 2009.